Supporting Information

Alkali metal hydroxides-treatment enhances the selectivity of $CdWO_4$ for oxygen reduction to hydrogen peroxide

Qi Wang[a, #], Fan Zhang[b, #], Hui Chen[a], Chuanchuan Fu[a], Yafei Wang[a], Ziyan Li[a], Junming Luo[a, *], Tianyu Qiu[a, *], Zhengpei Miao[a], Jing Li[a, *], and Zhitong Wang[a, *]

[a]*School of Marine Technology and Equipment, State Key Laboratory of Tropic Ocean Engineering Materials and Materials Evaluation, School of Chemistry and Chemical Engineering, Hainan Provincial Key Lab of Fine Chemistry, Hainan University, Haikou 570228, China*

[b]*State Power Investment Group Hainan Electric Power Co. Ltd., Haikou 570100, China*

[#]*These authors contributed equally to this work*

**Corresponding authors: Jumming Luo (luojunming@hainanu.edu.cn), Tianyu Qiu (qiuty@hainanu.edu.cn), Jing Li (jli@hainanu.edu.cn), and Zhitong Wang (zhitongwang@hainanu.edu.cn)*

Table of contents

1 Experimental section

1.1 Synthesis of catalysts

Synthesis of $CdWO_4$. In a typical synthesis, 2 mmol of $NaWO_4$ and 4 mmol of CTAB were dissolved in 40 mL of deionized water and stirred for 30 min to form solution A. 3 mmol of $Cd(NO_3)_2 \cdot 4H_2O$ was dissolved in 20 mL of deionized water and stirred for 30 min to form solution B. Solution A and solution B were mixed together, stirred for1 h, then transferred into a 100 mL stainless steel reactor. The reactor was put into an oven and kept 180 ℃ for 12 h. After cooling down room temperature, the white products in the reactor were washed with deionized water for 5 times and dried at 70 ℃ for 12 h to obtain the as-prepared $CdWO_4$ samples.

Synthesis of $CdWO_4$-MOH. The as-prepared $CdWO_4$ samples were soaked into 15 ml of 0.1 M MOH (M = Li, Na, K, Cs) aqueous solution to undergo the alkali metal hydroxides-treatment for 48 h. After that, the treated samples were collected by centrifugation, washed with deionized water for 5 times, and dried at 70 ℃ for 12 h to obtain the $CdWO_4$-MOH samples.

1.2 Characterization of catalysts

X-ray diffraction (XRD) was conducted on a DX-2700BH powder diffractometer operated at 40 kV and 40 mA, using Cu Kα radiation sources. Transmission electron microscopy (TEM), high-angle annular dark field (HAADF), and energy dispersive spectrometer (EDS) elemental mapping analysis were performed on a FEI Talos F200S microscope. X-ray photoelectron spectroscopy (XPS) was conducted on a thermo Scientific K-Alpha X-ray photoelectron spectrometer, employing monochromated Al Kα X-ray sources. The XPS data calibration was assisted by the adventitious carbon peak in the C 1s spectrum which was corrected to 284.8 eV. Brunauer-Emmett-Teller (BET) surface area of the samples were measured by N_2 adsorption at 77K with a BELSORP MAX X sorption system. In situ Fourier transform infrared (FT-IR) spectra were collected by an IRTracer-100 spectrometer. Concentration analysis of H_2O_2 was performed on an SHIMADZU UV-2700i ultraviolet-visible (UV-VIS) spectrophotometer.

1.3 Evaluation of catalysts

ORR performance and H_2O_2 selectivity tests were conducted on an electrochemical workstation (Autolab PGSTAT302N, Netherlands) at room temperature, using a three-electrode cell with a rotating disk electrode (RDE) system. An Hg/HgO electrode was used as the reference electrode in acid media. A graphite rod and a rotating ring disk electrode (RRDE, 0.180 cm^2 Pt ring, 0.247 cm^2 GC disk) were used as the counter electrode and the working electrode, respectively. All potentials in the text were quoted with respect to the reversible hydrogen electrode (RHE).

The preparation procedure of catalyst-loaded RRDE was as follows. First, 1 mL of a 0.25 wt % Nafion ethanol solution, 4 mg of the prepared catalyst, and 1 mg of carbon black (Cabot, XC-72) were mixed via ultrasonication for 40 min to form a catalyst ink. Then, 25.2 μL of the catalyst ink was pipetted onto the GC disk of RRDE. Finally, the catalyst-loaded RRDE was dried under an infrared lamp for 10 min. Loadings of the prepared catalysts in RRDE were 0.408 mg cm^{-2}.

The ORR performance of the catalysts was evaluated by linear sweep voltammetry (LSV) with a scanning rate of 10 mV/s in 0.1 M KOH solution. Cyclic voltammetry (CV) tests were scanned from 0.1 ~ 0.7 V vs. RHE with a scanning rate of 100 mV/s. In RRDE tests, the Pt ring was polarized at 1.4 V vs RHE. The electron-transfer number (n) was calcualted by $n = 4I_{disk} / (I_{disk} + (I_{ring}/N))$ and the H_2O_2 yield was calculated by H_2O_2 (%) $= (200I_{ring}/N) / (I_{disk} + (I_{ring}/N))$, where I_{disk} and I_{ring} were the absolute value of the disk current and ring current, respectively, and N was the collection efficiency ($N = 0.37$).

CV tests at various scan rates (10, 20, 30, 40, 50 mV/s) in a non-faradaic region (1.1 ~ 1.2 V vs. RHE) were carried out to calculate the double layer capacitance (C_{dl}) and electrochemical surface area (ECSA). C_{dl} was calculated by $C_{dl} = \Delta(j_a - j_c) / 2\Delta v$, where j_a, j_c, and v represent a specified anodic current density, a specified cathodic current density at the same potential, and the corresponding scan rate. ECSA was calculated by ECSA $= C_{dl} / C_s$, where C_s represent the specific capacitance, which is estimated as 40 μF cm^{-2} according to previous literature.[1]

1.4 Flow cell tests

The flow cell tests were conducted on a gas diffusion electrolytic cell (Gaossunion, 101016), which consists of a catalyst-loaded carbon paper as the cathode, a Pt foil as the anode, and an anion exchange membrane (Sinero, FAS-PET-130). The preparation procedure of catalyst-loaded carbon paper was as follows. In a typical procedure, 1 mL of a 0.25 wt % Nafion ethanol solution, 40 mg of the prepared catalyst, and 10 mg of carbon black (Cabot, XC-72) were mixed via ultrasonication for 40 min to form a catalyst ink. Then, 300 μL of the catalyst ink was pipetted onto the carbon paper (3 cm^2). Finally, the catalyst-loaded carbon paper was dried under an infrared lamp for 20 min. Without specified, loadings of the prepared catalysts in RRDE were 4 mg cm^{-2}. The active area of the catalyst-loaded carbon paper in flow cell tests was 1 cm^2.

During flow cell tests, 30 mL of 1 M KOH solution was used as the catholyte and the anolyte, respectively, which was agitated into the cathode and anode of the flow cell at a flow rate of 15 mL min^{-1} with the assistance of a peristaltic pump. O_2 as the reactants of the cathode was fed with a flow rate of 25 mL min^{-1}. Stability tests in flow cells were conducted by constantly discharging at 100 mA cm^{-2}. The catholyte was sampled and replaced every 2 h in stability tests.

The Faradaic efficiency (FE) of H_2O_2 production in flow cell tests was calculated by Eq. (1), where $n_{H_2O_2}$ is the mole of H_2O_2, N_A is the Avogadro constant, e is the electron, I is the applied current, t is the sampling time.

$$FE = 100\% \times 2 \times n_{H_2O_2} \times N_A \times e / (I \times t) \quad (1)$$

1.5 Determination of H_2O_2

A spectroscopic titration using $Ce(SO_4)_2$ as an indicator was employed to determine the concentration of H_2O_2. The mechanism of this method is that yellow Ce^{4+} can be reduced to colorless Ce^{3+} by H_2O_2 (Eq. (2)).

$$2Ce^{4+} + H_2O_2 \rightarrow 2Ce^{3+} + 2H^+ + O_2 \quad (2)$$

The amount of consumed Ce^{4+} in the reaction can be determined by UV-VIS spectrophotometry. The absorbance at 316 nm was used to calculate the amount of consumed Ce^{4+}. Therefore, the amount of H_2O_2 can be calculated by $n(H_2O_2) = 0.5 \times n(Ce^{4+})$, where $n(H_2O_2)$ is the mole of H_2O_2 and $n(Ce^{4+})$ is the mole of

consumed Ce^{4+}.

The calibration curve for H_2O_2 determination was obtained by adding known H_2O_2 solutions into the solutions containing 1 mM $Ce(SO_4)_2$ and 0.5 M H_2SO_4 and measuring the absorbance (Abs) at 316 nm (denoted as A_S). The obtained calibration curve in Figure S22 shows that Abs followed a good linear relation with the amount of H_2O_2. For the determination of H_2O_2 in flow cells, we sample a certain amount of catholyte, measure its absorbance, and calculate the Abs value. Then, the amount of H_2O_2 produced in flow cells was calculated based on the linear relation in the calibration curve. The determination of H_2O_2 in stability tests and at different discharging current density was sampled 3 times.

1.6 Computational details

DFT calculations were performed using the Perdew-Burke-Ernzerhof (PBE) functional and the projector augmented wave (PAW) potential as implemented in the Vienna Ab Initio Simulation Package (VASP). An energy cutoff of 450 eV and a convergence criterion of 10-5 eV for self-consistent calculations was adopted. All structures were fully relaxed until the total force on each atom was less than 0.05 eV/Å. $CdWO_4$ and Cs-doped $CdWO_4$ ($CsCdWO_4$) were set to gamma k-point was adopted during the constructure optimization, and $3 \times 3 \times 1$ k-point was employed during the electronic structure calculations. The DFT-D3 method with Becke-Jonson damping is used to add vdW dispersion correction.

2 Supplementary Figures S1-S22 and Tables S1-S2

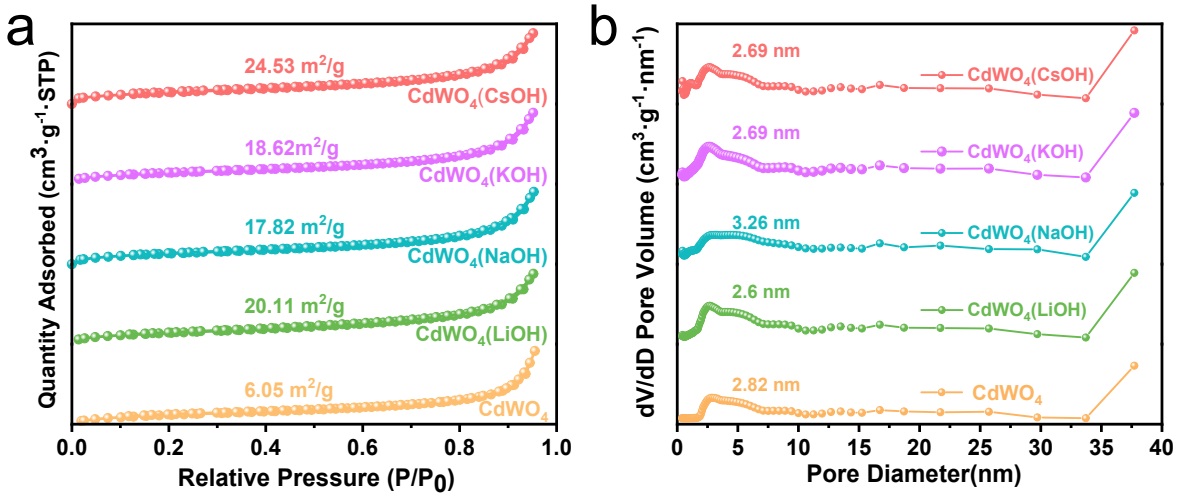

Figure S1. (a) N_2 adsorption–desorption isotherms of the $CdWO_4$ and $CdWO_4$-MOH catalysts. (b) Pore distribution of the $CdWO_4$ and $CdWO_4$-MOH catalysts.

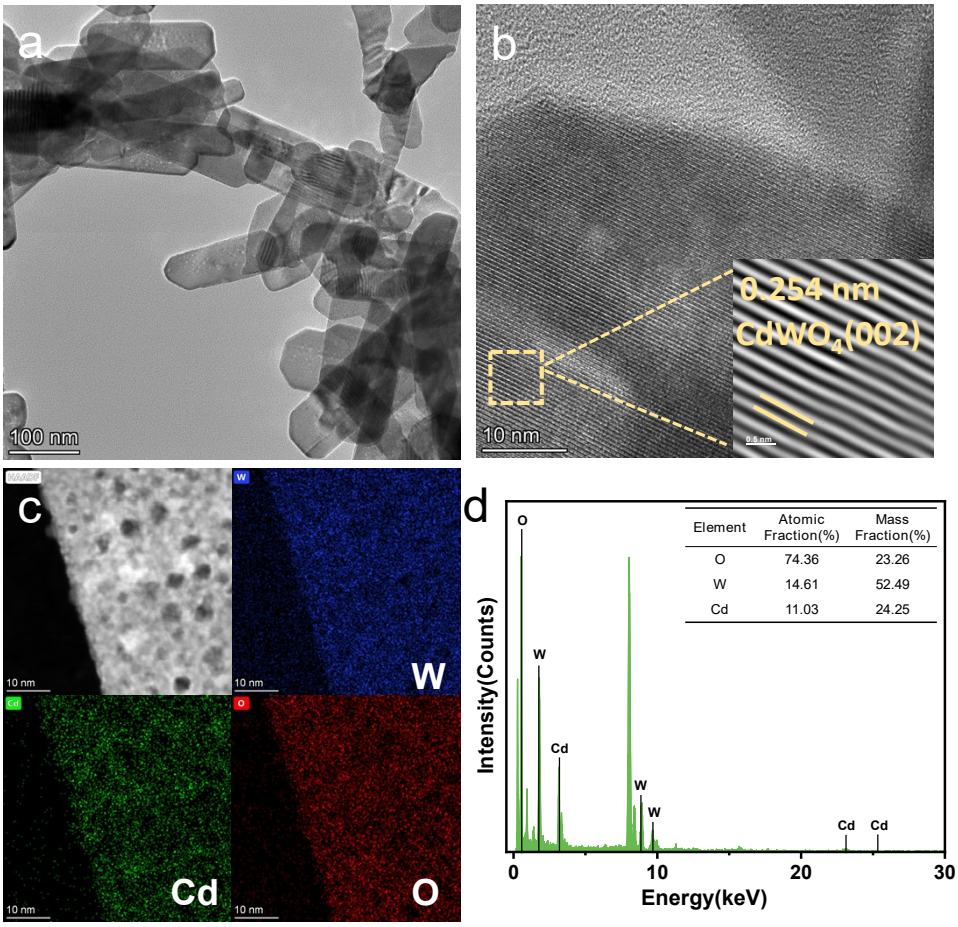

Figure S2. (a, b) TEM image of the $CdWO_4$ catalyst. (c) HAADF and EDS mapping images of the $CdWO_4$ catalyst. (d) EDX profile of the $CdWO_4$ catalyst.

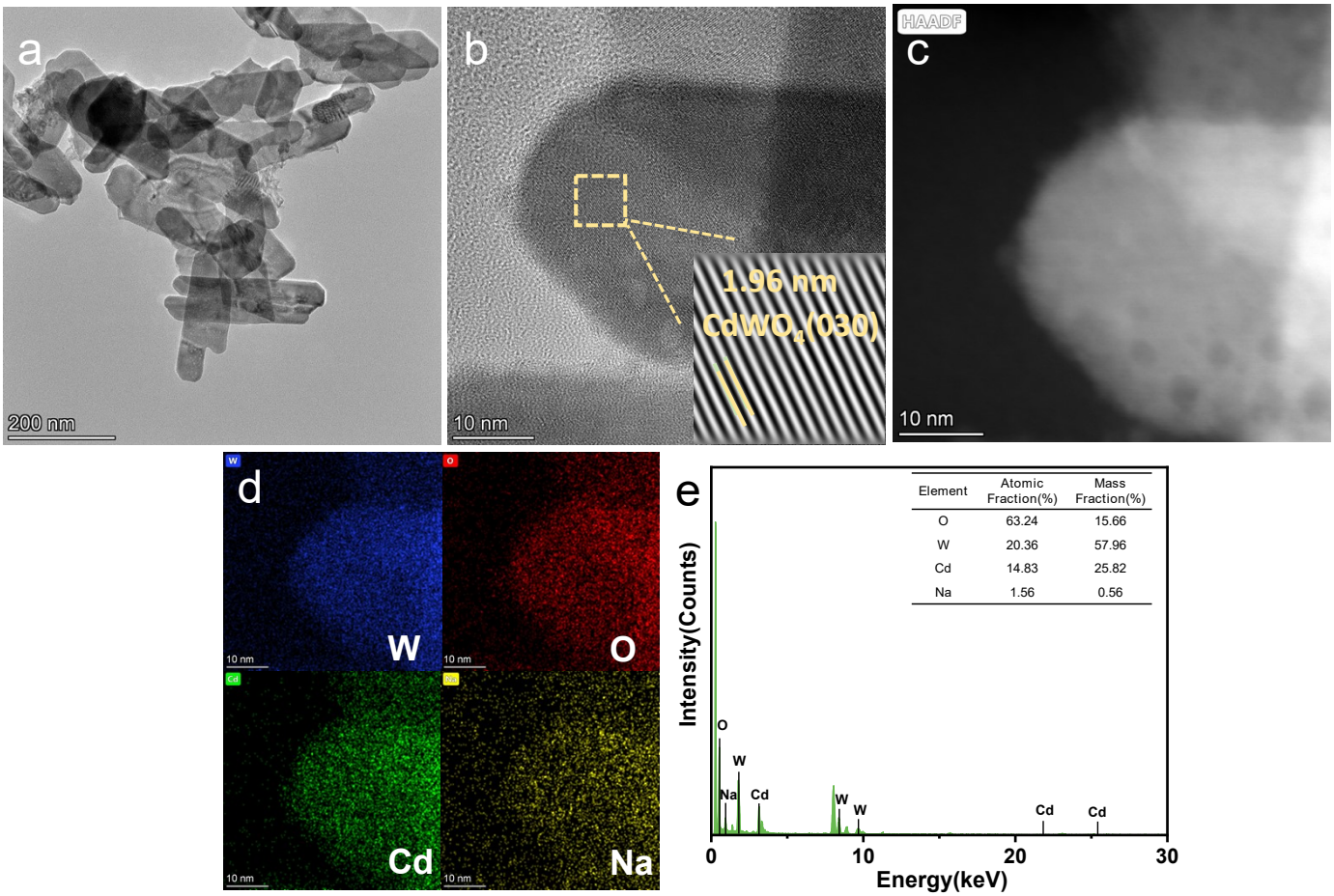

Figure S3. (a, b) TEM image of the $CdWO_4$-NaOH catalyst. (c, d) HAADF and EDS mapping images of the $CdWO_4$-NaOH catalyst. (e) EDX profile of the $CdWO_4$-NaOH catalyst.

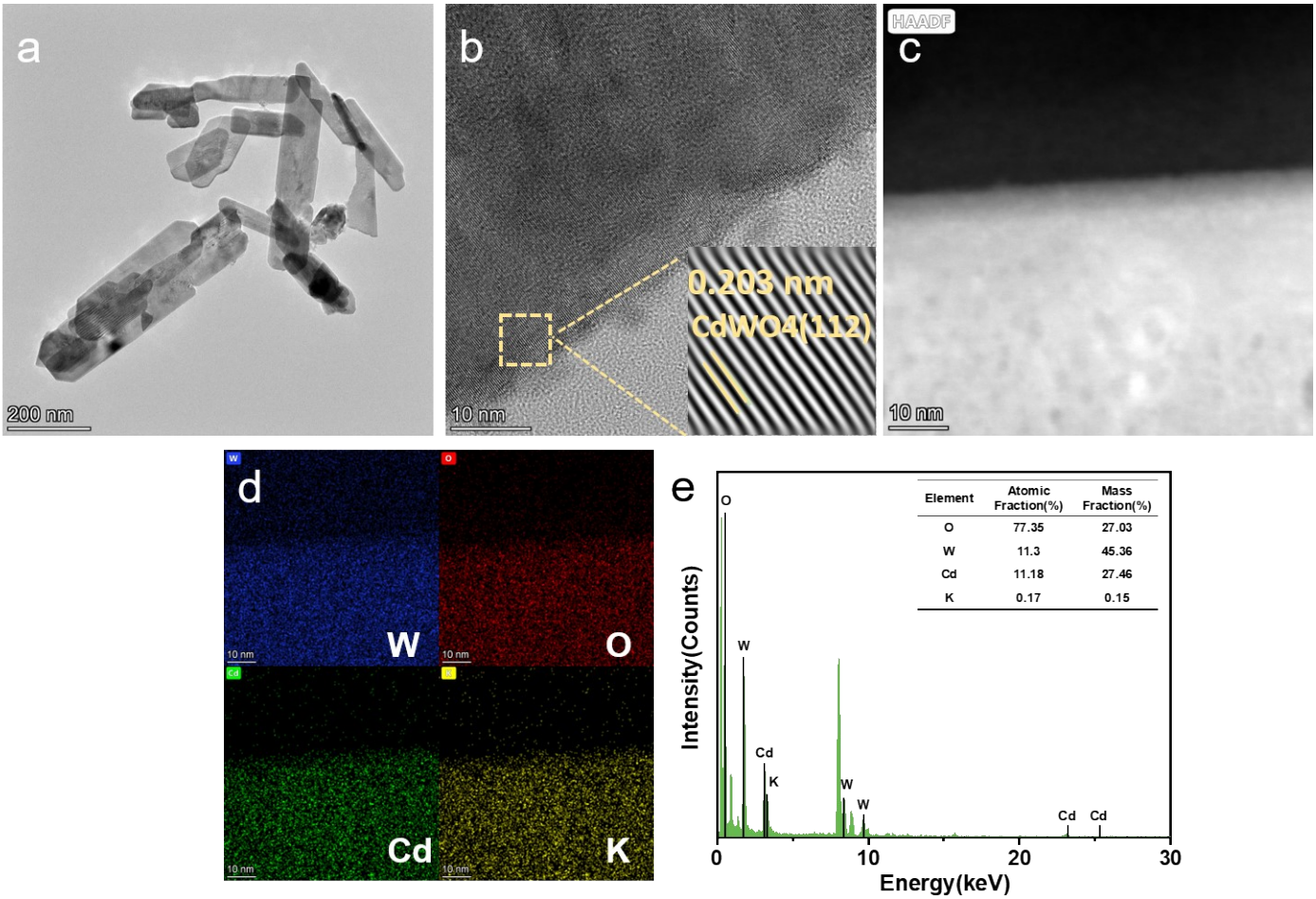

Figure S4. (a, b) TEM image of the $CdWO_4$-KOH catalyst. (c, d) HAADF and EDS mapping images of the $CdWO_4$-KOH catalyst. (e) EDX profile of the $CdWO_4$-KOH catalyst.

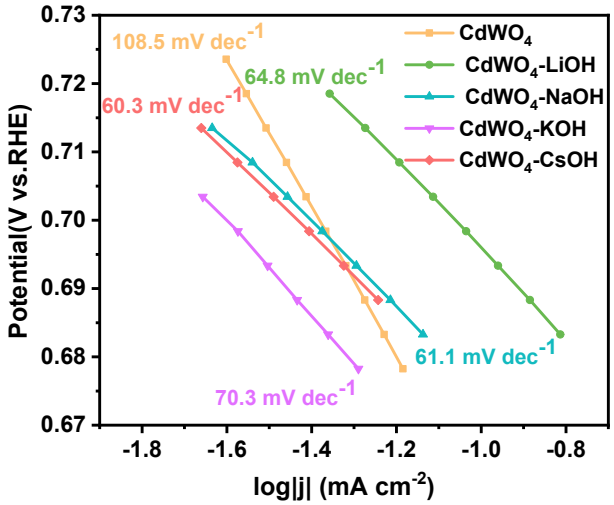

Figure S5. Tatal slopes of the $CdWO_4$ and $CdWO_4$-MOH catalysts.

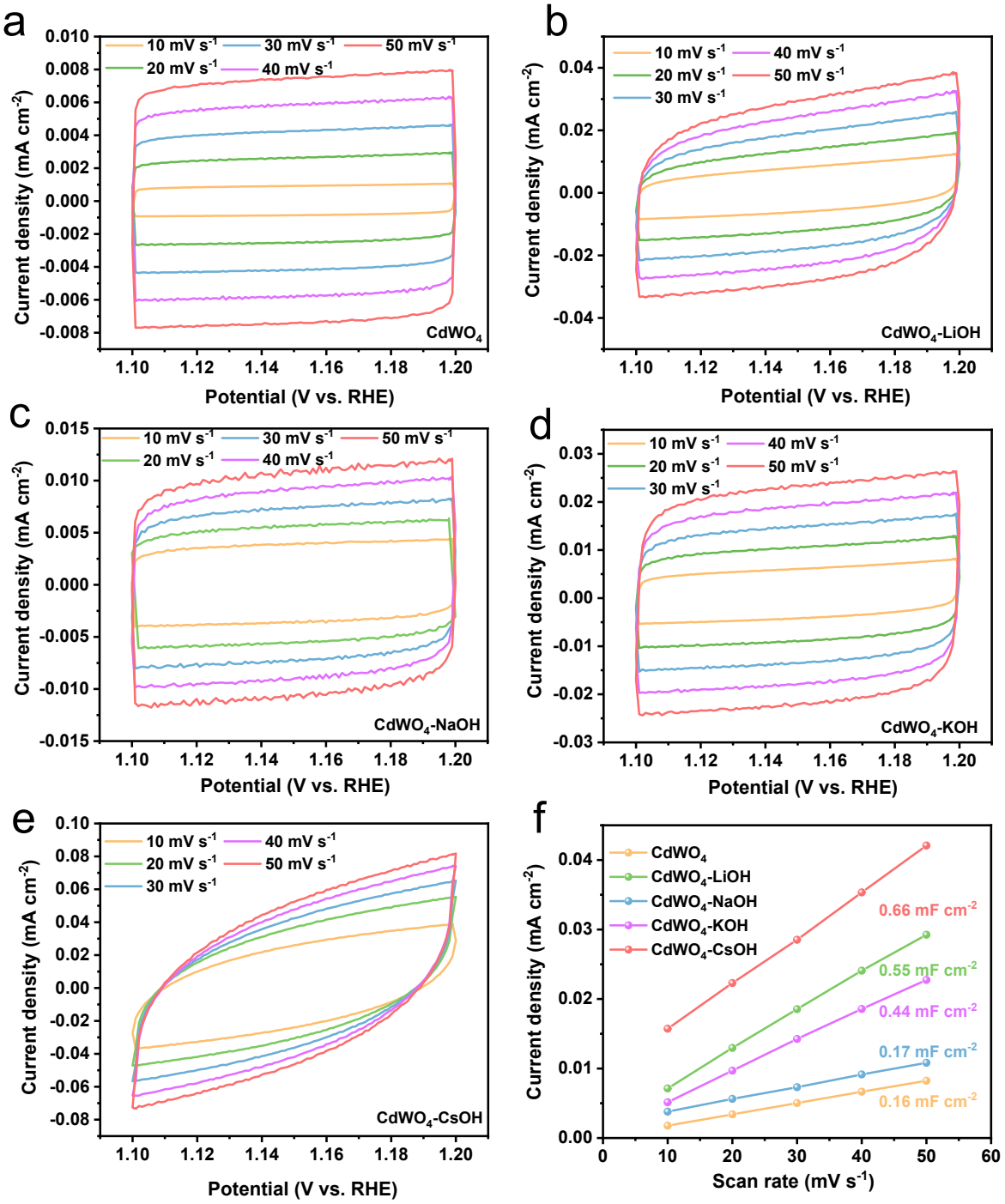

Figure S6. (a-e) CV curves of $CdWO_4$-MOH at various scan rates in non-faradaic region. (f) The estimated C_{dl} of $CdWO_4$-MOH.

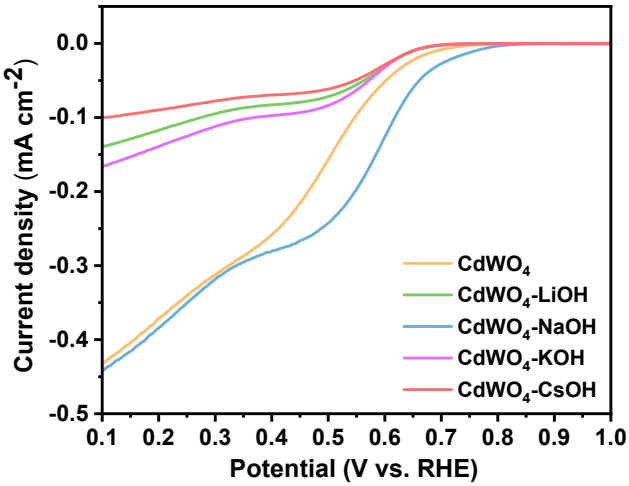

Figure S7. ECSA-normalized ORR activity of $CdWO_4$-MOH. The calculated ECSAs of $CdWO_4$, $CdWO_4$-LiOH, $CdWO_4$-NaOH, $CdWO_4$-KOH, and $CdWO_4$-CsOH were 4.00, 13.75, 4.25, 11.00, and 16.50 cm^{-2}, respectively.

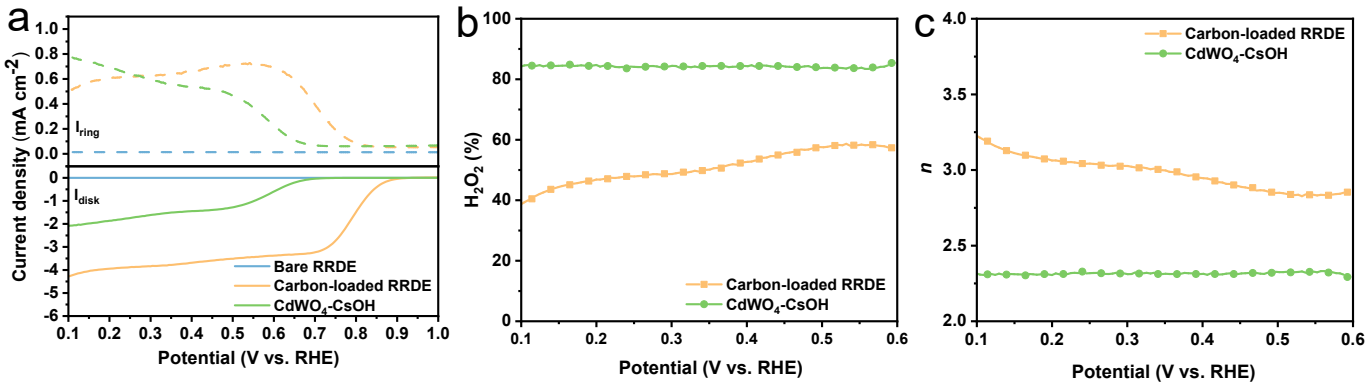

Figure S8. ORR performance of bare RRDE, carbon-loaded RRDE and $CdWO_4$-CsOH in 0.1 M KOH solution. (a) LSV curves in O_2-saturated 0.1 M KOH solution, solid line and dashed line represent disk current density and ring current density, respectively, 1600 rpm. (b) H_2O_2 selectivity in RRDE tests. (c) *n* in RRDE tests.

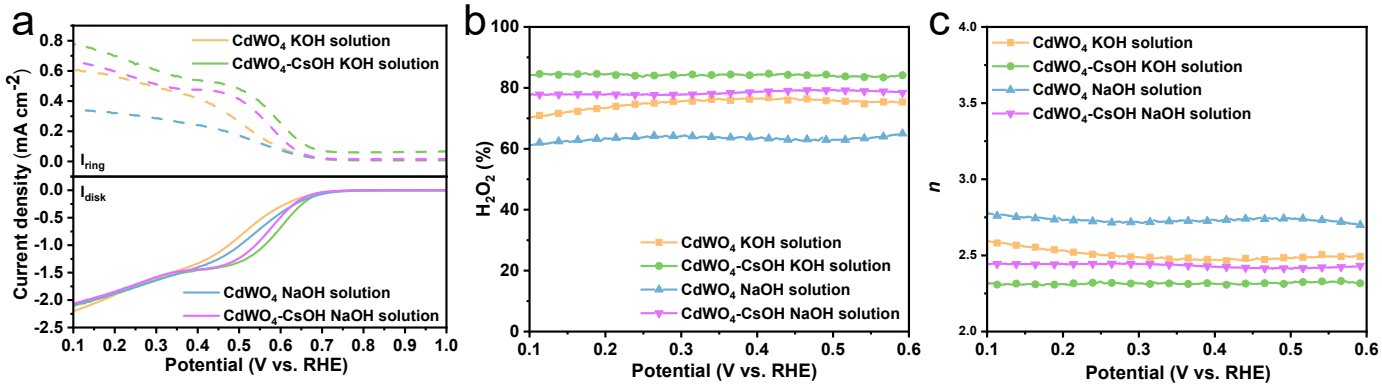

Figure S9. Comparison of the ORR performance of $CdWO_4$ and $CdWO_4$-CsOH in 0.1 M KOH and NaOH solutions. (a) LSV curves, solid line and dashed line represent disk current density and ring current density, respectively, 1600 rpm. (b) H_2O_2 selectivity in RRDE tests. (c) *n* in RRDE tests.

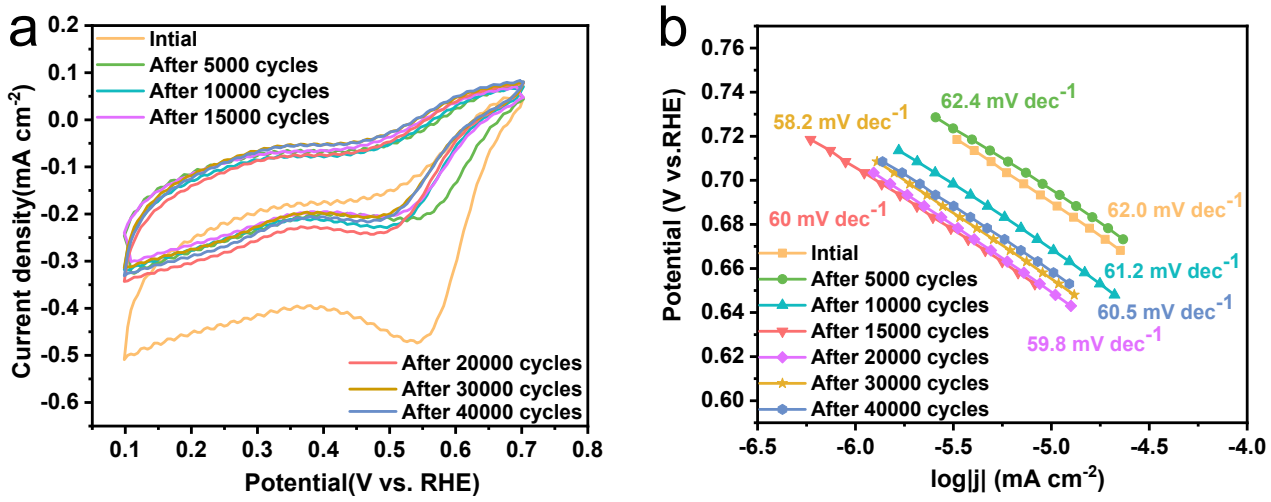

Figure S10. (a) CV curves of the $CdWO_4$-CsOH catalyst after CV cycles. (b) Tafel slopes of the $CdWO_4$-CsOH catalyst after CV tests.

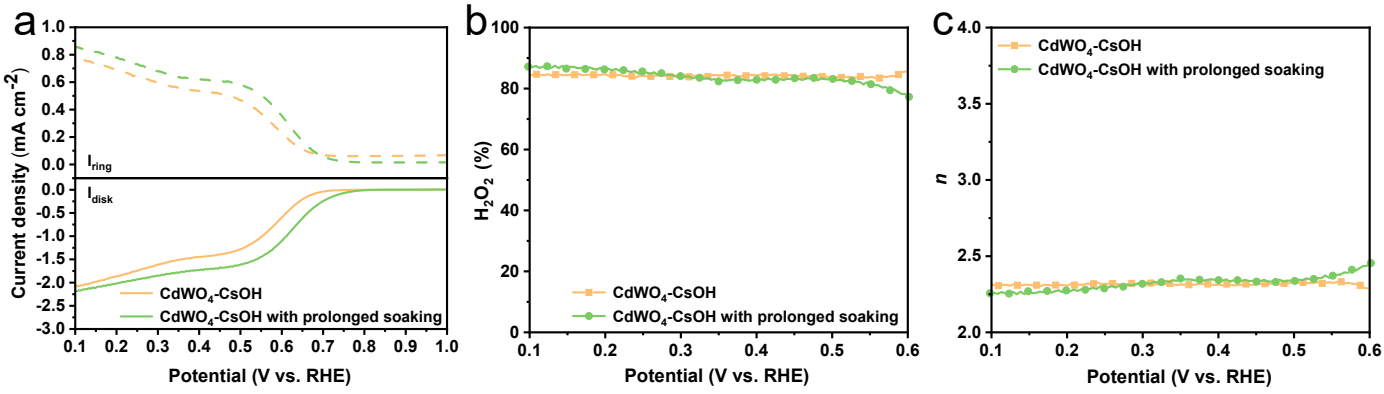

Figure S11. Comparison of the ORR performance of $CdWO_4$-CsOH with and without prolonged soaking in

0.1 M KOH solution. (a) LSV curves in 0.1 M KOH solution, solid line and dashed line represent disk current density and ring current density, respectively, 1600 rpm. (b) H_2O_2 selectivity in RRDE tests. (c) *n* in RRDE tests. The prolonged soaking time in 0.1 M KOH solution equals the time of the 40,000 CV cycles in 0.1 M KOH solution.

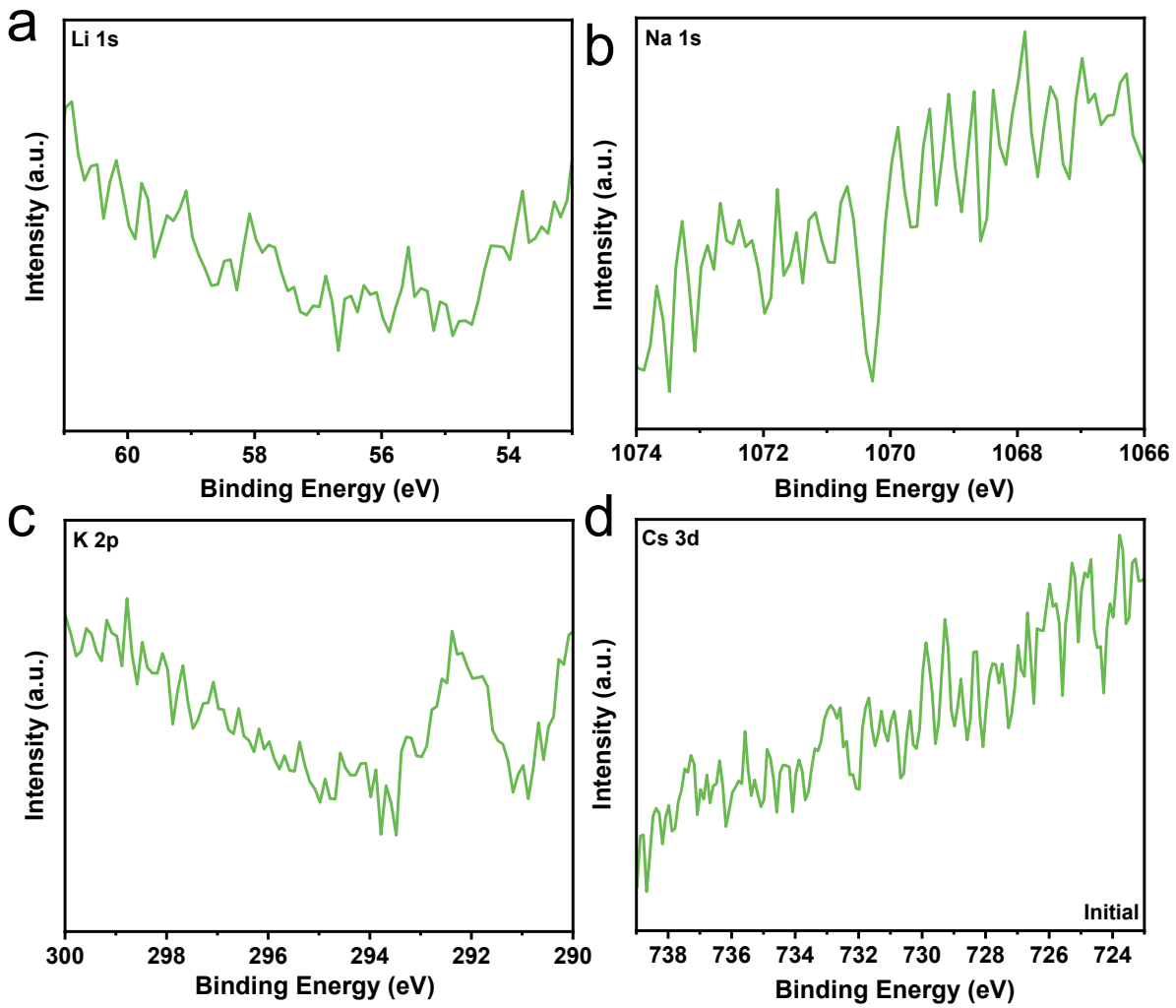

Figure S12. (a) XPS spectrum of Li 1s in $CdWO_4$-LiOH. (b) XPS spectrum of Na 1s in $CdWO_4$-NaOH. (c) XPS spectrum of K 2p in $CdWO_4$-KOH. (d) XPS spectrum of Cs 3d in $CdWO_4$-CsOH.

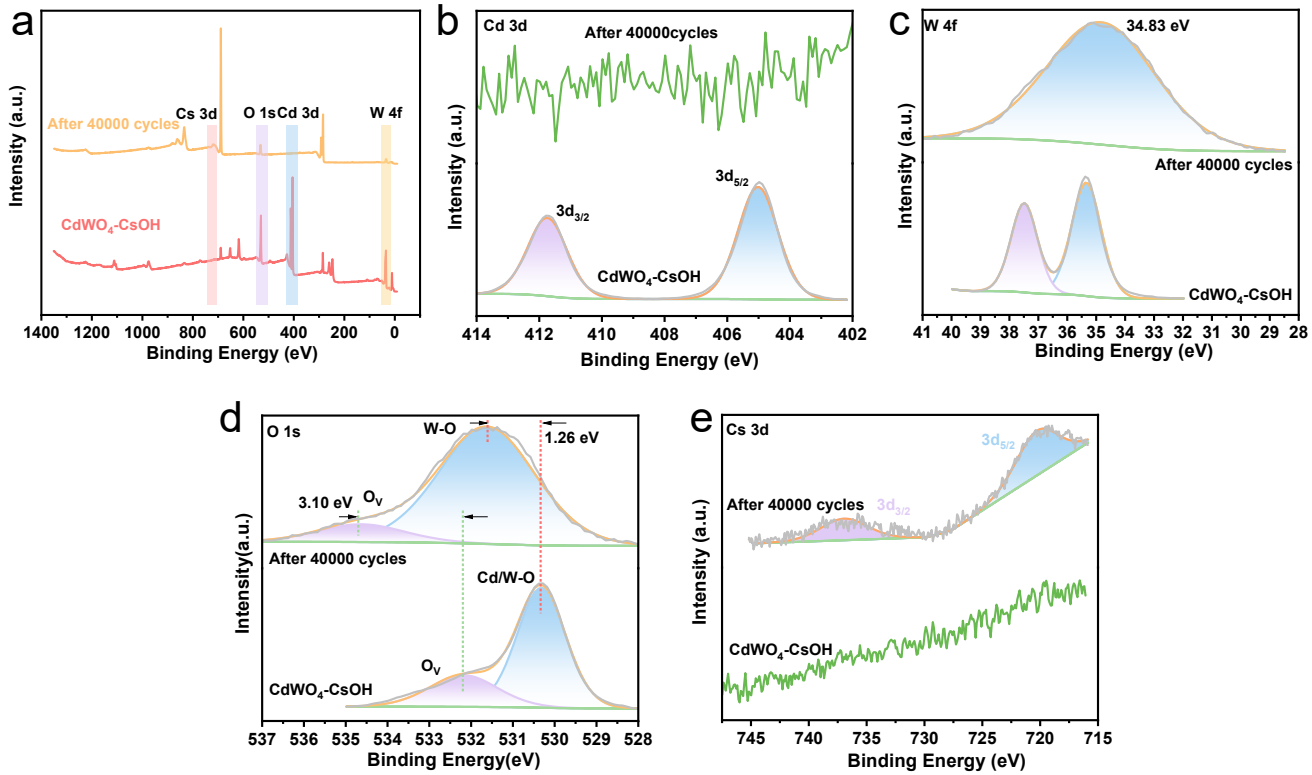

Figure S13. XPS analysis of $CdWO_4$-CsOH before and after 40,000 CV cycles. (a) XPS survey spectra. (b) XPS spectra of Cd 3d. (c) XPS spectra of W 4f. (d) XPS spectra of O 1s. (e) XPS spectra of Cs 3d.

It should be mentioned that the absence of detectable Cs signals before the CV test is caused by the extremely low content of Cs in the surfaces of $CdWO_4$-CsOH which is under the limit of detection of the XPS analyzer.

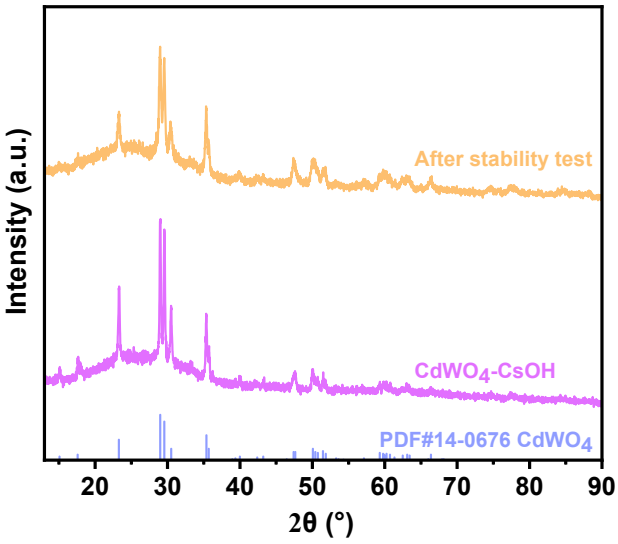

Figure S14. XRD patterns of $CdWO_4$-CsOH before and after 40,000 CV cycles.

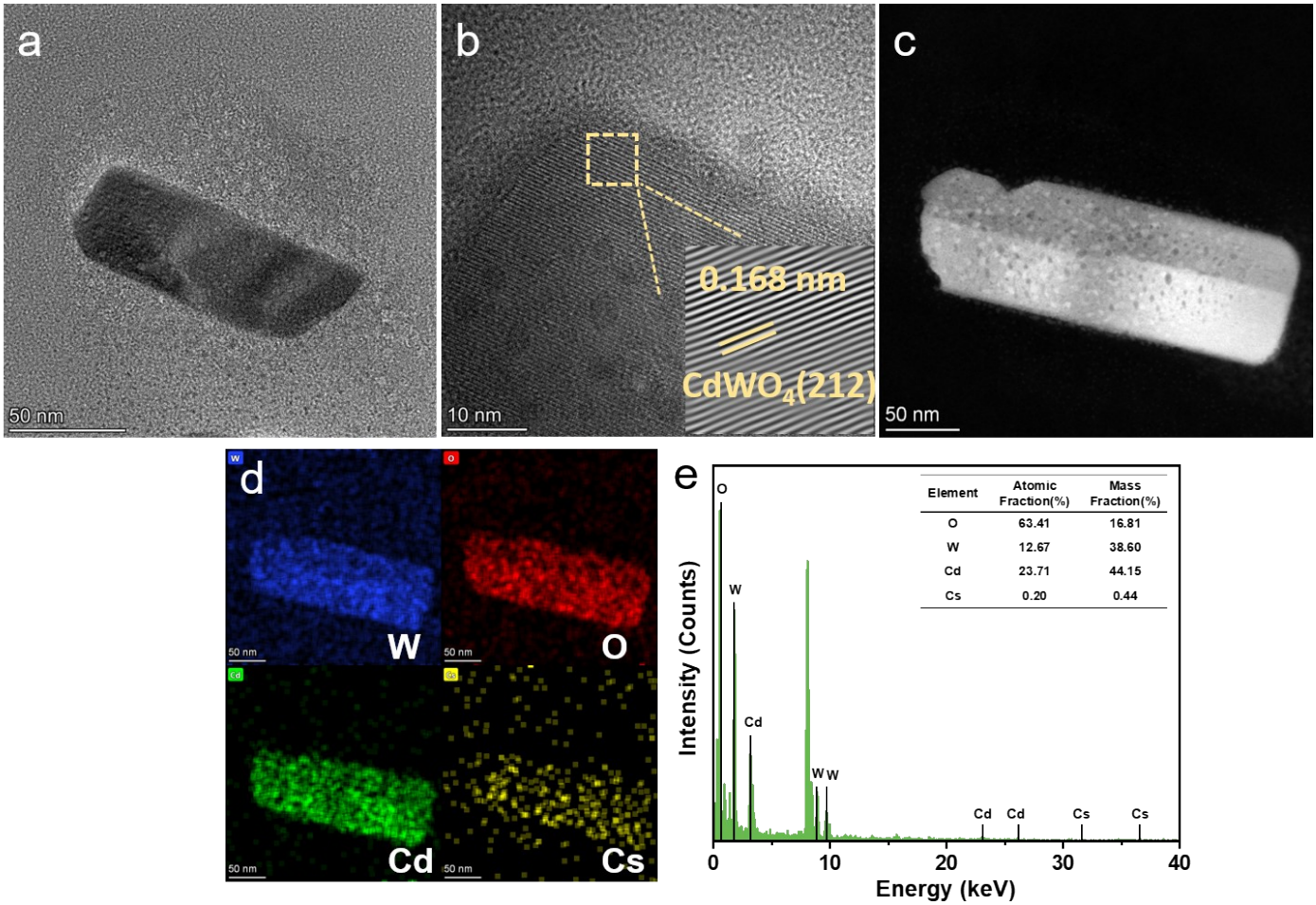

Figure S15. (a, b) TEM image of the $CdWO_4$-CsOH catalyst after stability test. (c, d) HAADF and EDS mapping images of the $CdWO_4$-CsOH catalyst after stability test. (e) EDX profile of the $CdWO_4$-CsOH catalyst after stability test.

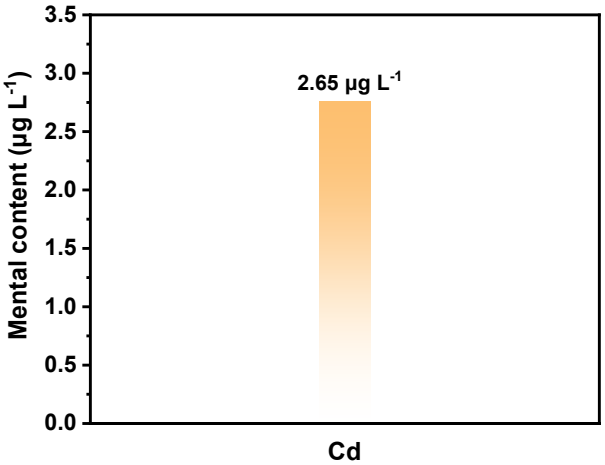

Figure S16. The content of dissolved Cd from $CdWO_4$-CsOH in the electrolyte after 40,000 CV cycles.

After the long-term CV tests, the electrolyte contained 2.65 μg L^{-1} of Cd, which is lower than the limit line (3.0 μg L^{-1}) of World Health Organization.

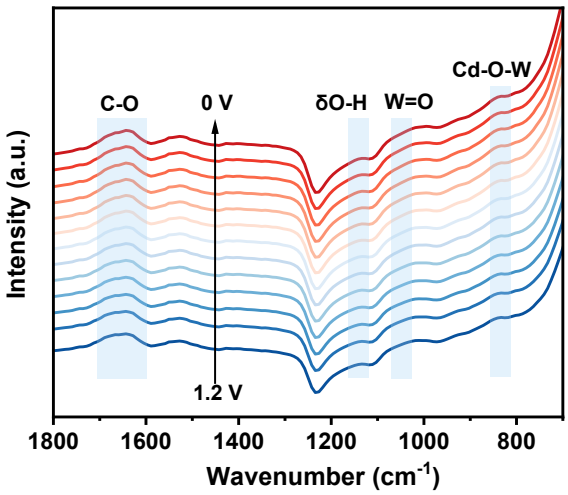

Figure S17. In situ FT-IR spectra of $CdWO_4$-CsOH catalysts scanning from 1.2 to 0 V vs. RHE in Ar-saturated 0.1 M KOH solution.

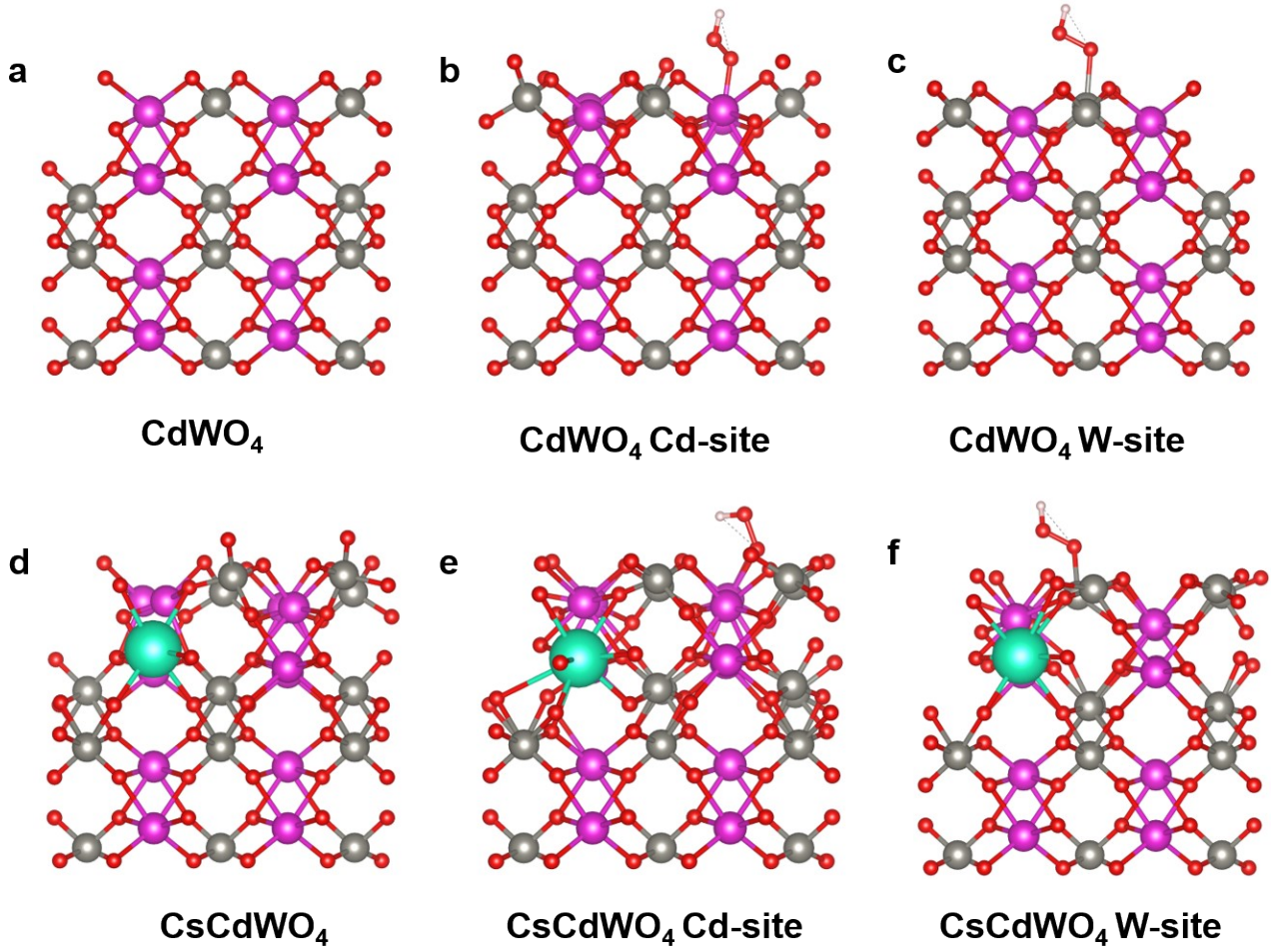

Figure S18. (a-c) A schematic illustration of the $CdWO_4$ model and the optimized adsorption configurations of OOH on the Cd and W sites on the exposed $CdWO_4$ (100) surface. (d-f) A schematic illustration of the $CsCdWO_4$ model and the optimized adsorption configurations of OOH on the Cd and W sites on the exposed

$CsCdWO_4$ (100) surface. Purple, grey, cyan, red, and white spheres denotes Cd, W, Cs, O, and H atoms, respectively.

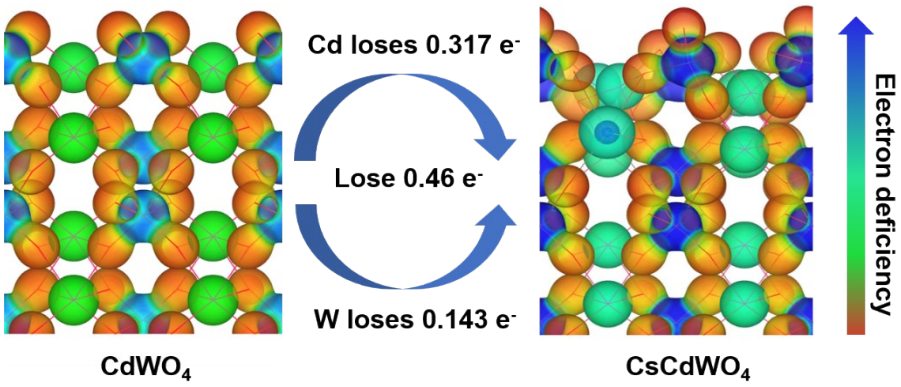

Figure S19. Charge density distribution in $CdWO_4$ and $CsCdWO_4$ models. Compared to $CdWO_4$, the $CsCdWO_4$ model totally loses 0.46 e^-, among which Cd atoms lose 0.317 e^- and W atoms lose 0.143 e^-.

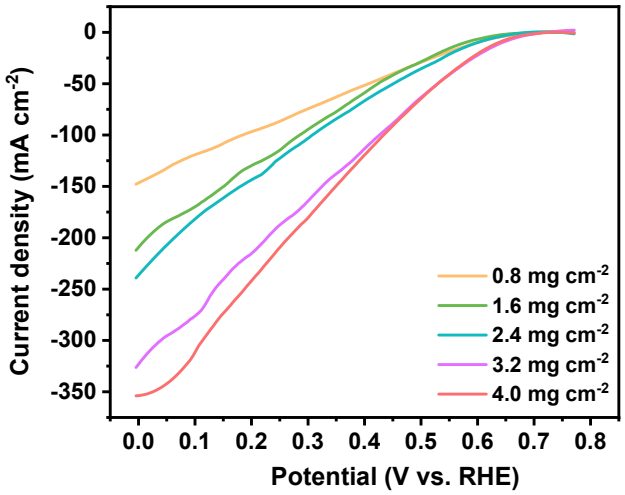

Figure S20. Polarization curves of the flow cell with different loading of $CdWO_4$-CsOH.

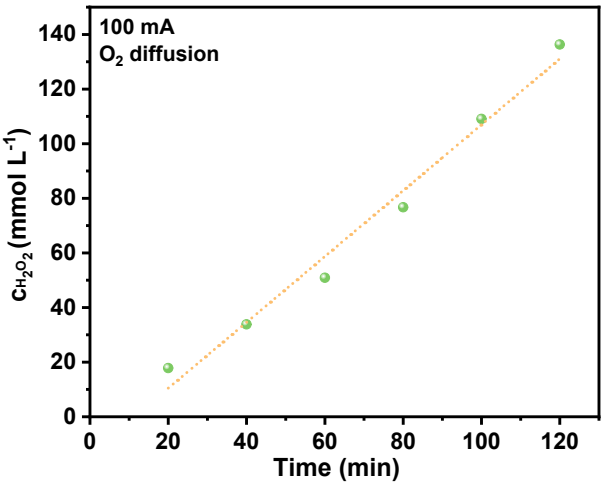

Figure S21. The accumulation of H_2O_2 concentration within 2 h test in the flow cell.

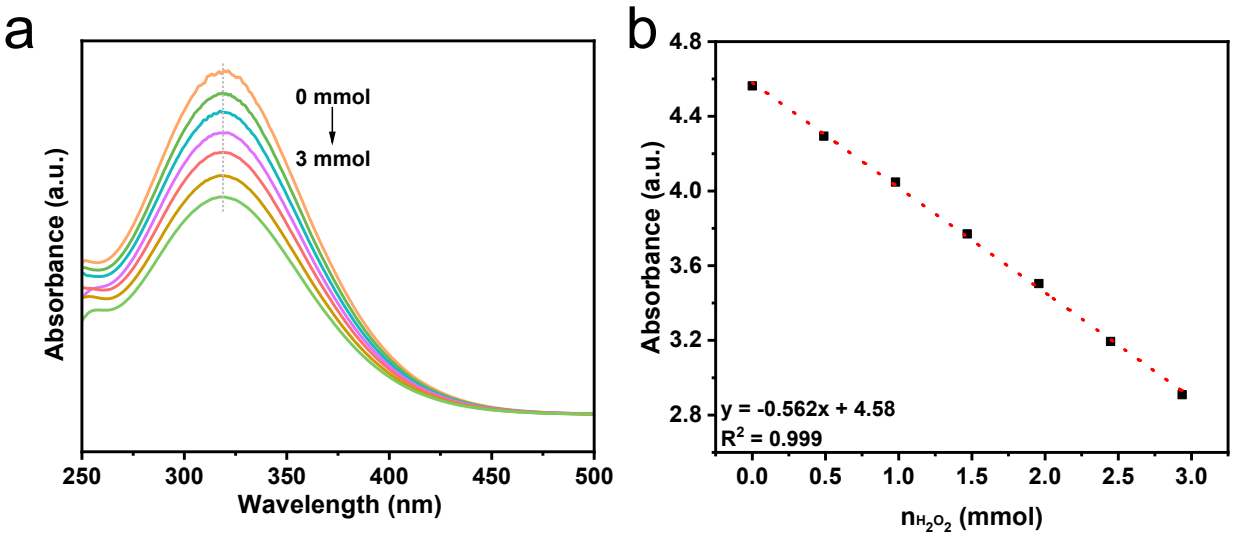

Figure S22. H_2O_2 determination were measured by titration using solutions containing 1 mM $Ce(SO_4)_2$ and 0.5 M H_2SO_4. (a) Absorption spectra of the solutions containing 1 mM $Ce(SO_4)_2$ and 0.5 M H_2SO_4 with the different addition of H_2O_2 (0, 0.5, 1, 1.5, 2, 2.5, 3 mmol). (b) Plot of Abs at λ = 318 nm as a function of the mole of H_2O_2.

Table S1. Performance list of transition metal oxides and other types of representative catalysts for H_2O_2 production via $2e^-$ ORR in alkaline solution.

Catalyst	Electrolyte	Onset potential (V vs. RHE)	H_2O_2 Selectivity (%)	Current density (mA cm^{-2})	FE in flow cells (%)	Test time (h)	H_2O_2 production rate (mmol cm^{-2} h^{-1})	Ref.
$CdWO_4$-CsOH	0.1 M KOH	**0.68**	**84.3**	**100**	**84.3 (77.3~ 90.9)**	**34**	**1.72**	**This work**
$CdWO_4$-CsOH after 15000 CV cycles		**0.64**	**94.7**					
$CdWO_4$-CsOH after 40000 CV cycles		**0.62**	**93.7**					
Nb_2O_5-rGO	0.1 M NaOH	-0.22 (Ag/AgCl)	74.9	-	-	-	-	2
CoxOy/C	1 M NaOH	-0.10 (Hg/HgO)	74	-	-	-	-	3
4% CeO_2/C	1 M NaOH	-0.12 (Hg/HgO)	88	-	-	-	-	4
Fe_3O_4/Printex	1 M KOH	0.28 (SCE)	68	-	-	-	-	5
Fe_3O_4/graphene	1 M KOH	0.22 (SCE)	62	-	-	-	-	5
Cu/C-700_{EC}	0.1 M KOH	~0.53	68	-	-	-	-	6
Co-N_3O	0.1 M KOH	0.85	~90	110	~75	12	0.284	7
Ni-N_3S	0.1 M KOH	0.75	~85	110	~85	12	0.350	7

ZnO; CuO; NiO; CoO	0.1 M KOH	0.52; 0.50; 0.51; 0.45	90; 82.8; 79.4; 36.8	-	-	-	-	8
utn-NiBDC	0.1 M KOH	~0.61	~ 90	200	~ 80	100	3.425	9
SC-COF_{TSA}	0.1 M KOH	~0.66	~ 99	400	~ 95	50	14.1	10
Zn-NiO; Fe-NiO; NiO	0.1 M KOH	~0.58 ~0.58; ~0.57	93; 91; 84	-	-	-	-	11
$BiOS_{SA}/Bi_{clu}$	0.1 M KOH	~0.68	~ 90	~5 (H-cell)	88	22	0.30	12
O-CNTs	0.1 M KOH	~0.61	~ 90	-	-	-	-	13
P-NMG-10	0.1 M KOH	~0.73	＞80	~80	80~90	24	1.20	14
Co-HSACs	0.1 M KOH	~0.76	~ 95	300	~ 90	25	-	15
Mn-NO-C_H	0.1 M KOH	0.68	＞87	~120	＞96	55	2.416	16
Pb SA/OSC	0.1 M KOH	0.61	~90	50	＞92	100	6.9	17
Pd SNCs/$NiTe_2$	0.1 M KOH	0.81	99	100	95	10	1.75	18

Table S2. Atomic contents of the $CdWO_4$, $CdWO_4$-MOH catalysts in XPS analysis.

Sample	Atomic content (%)						
	O	W	Cd	Li	Na	K	Cs
$CdWO_4$	64.06	15.30	20.64	-	-	-	-
$CdWO_4$-LiOH	63.04	11.85	15.73	9.37	-	-	-
$CdWO_4$-NaOH	70.62	12.25	16.66	-	0.47	-	-
$CdWO_4$-KOH	69.99	12.74	16.09	-	-	1.18	-
$CdWO_4$-CsOH	70.79	13.03	16.01	-	-	-	0.18
$CdWO_4$-CsOH (after 40000 CV cycles)	88.56	8.70	0.48	-	-	-	2.26

References

1. Y. Yuan, Q. Wang, Y. Qiao, X. Chen, Z. Yang, W. Lai, T. Chen, G. Zhang, H. Duan, M. Liu, H. Huang, *Adv. Energy Mater*., 2022, **12**, 2200970
2. J. F. Carneiro, M. J. Paulo, M. Siaj, A. C. Tavares and M. R. V. Lanza, *J Catal*, 2015, **332**, 51-61.
3. M. H. M. T. Assumpção, D. C. Rascio, J. P. B. Ladeia, R. F. B. De Souza, E. T. Neto, M. L. Calegaro, R. T. S. Oliveira, I. Gaubeur, M. R. V. Lanza and M. C. Santos, *Int J Electrochem Sc*, 2011, **6**, 1586-1596.
4. M. H. M. T. Assumpção, A. Moraes, R. F. B. De Souza, M. L. Calegaro, M. R. V. Lanza, E. R. Leite, M. A. L. Cordeiro, P. Hammer and M. C. Santos, *Electrochim. Acta*, 2013, **111**, 339-343.
5. W. R. P. Barros, Q. Wei, G. Zhang, S. Sun, M. R. V. Lanza and A. C. Tavares, *Electrochim. Acta*, 2015,

162, 263-270.

6. B. Yu, J. Diniz, K. Lofgren, Q. Liu, R. Mercado, F. Nichols, S. R. J. Oliver and S. Chen, *ACS Sustain. Chem. Eng.*, 2022, **10**, 15501-15507.

7. W. Liu, R. Chen, Z. Sang, Z. Li, J. Nie, L. Yin, F. Hou and J. Liang, *Adv. Mater.*, 2024, **36**, 2406403.

8. Y. Zhang, H. Jiang, C. Zhang, Y. Feng, H. Feng, S. Zhu and J. Hu, *J. Mater. Chem. A*, 2024, **12**, 6123-6133.

9. T. Zhang, W. Wang, W. Liu, Z. Guo and J. Liu, *Nat. Commun.*, 2025, **16**, 5240.

10. J. Song, Z. Zhang, W. Li, C. Liu, G. Feng, Y. Su, K. Xi, H. Yi, C. Yi and L. Peng, *Nat. Commun.*, 2025, **16**, 8963.

11. H. Feng, Y. Song, Y. Zhang, Q. Qi, C. Zhang, Y. Feng and J. Hu, *Chem Eng J*, 2025, **506**, 160364.

12. P. Zhu, W. Feng, D. Zhao, P. Song, M. Li, X. Tan, T. Liu, S. Liu, W. Zhu, Z. Zhuang, J. Zhang and C. Chen, 2023, **135**, e202304488.

13. Z. Y. Lu, G. X. Chen, S. Siahrostami, Z. H. Chen, K. Liu, J. Xie, L. Liao, T. Wu, D. C. Lin, Y. Y. Liu, T. F. Jaramillo, J. K. Norskov and Y. Cui, *Nat. Catal.*, 2018, **1**, 156-162.

14. W. Peng, J. Liu, X. Liu, L. Wang, L. Yin, H. Tan, F. Hou and J. Liang, *Nat. Commun.*, 2023, **14**, 4430.

15. W. Fan, Z. Duan, W. Liu, R. Mehmood, J. Qu, Y. Cao, X. Guo, J. Zhong and F. Zhang, *Nat. Commun.*, 2023, **14**, 1426.

16. L.-Y. Dong, J.-S. Wang, T.-Y. Li, T. Wu, X. Hu, Y.-T. Wu, M.-Y. Zhu, G.-P. Hao and A.-H. Lu, *Angew. Chem. Int. Edit.*, 2024, **63**, e202317660.

17. X. Zhou, Y. Min, C. Zhao, C. Chen, M.-K. Ke, S.-L. Xu, J.-J. Chen, Y. Wu and H.-Q. Yu, *Nat. Commun.*, 2024, **15**, 193.

18. Y. Li, Y. Liu, X. Peng, Z. Zhao, Z. Li, B. Yang, Q. Zhang, L. Lei, L. Dai and Y. Hou, *Angew. Chem. Int. Edit*., 2024, **64**, e202413159.